

Raman Microprobe Analysis of Elastic Strain and Fracture in Electrophoretically Deposited CdSe Nanocrystal Films

Sarbajit Banerjee, Shengguo Jia, Dae I. Kim, Richard D. Robinson, Jeffrey W. Kysar, Joze Bevk, and Irving P. Herman*

Materials Research Science and Engineering Center, Columbia University, New York, New York 10027

Received September 28, 2005; Revised Manuscript Received November 23, 2005

ABSTRACT

The mechanical stability of nanocrystal films is critical for applications, yet largely unexplored. Raman microprobe analysis used here to probe the nanocrystal cores of thick, fractured electrophoretically deposited films of 3.2 nm diameter CdSe nanocrystals measures $\sim 2.5\%$ in-plane tensile strain in cores of unfractured films. The crack dimensions determine the overall in-plane film strain, $\sim 11.7\%$, and the film biaxial modulus, ~ 13.8 GPa, from which the biaxial modulus of the trioctylphosphine oxide ligand matrix is inferred, ~ 5.1 GPa.

Residual stress is common in films formed from solutions containing nanocrystals. Stress and strain build up when the solvent evaporates, seemingly because the nanocrystals adhere to the substrate and each other, even with some residual solvent present. Film fracture sometimes results for large stresses. In this Letter we show how Raman microprobe scattering from the CdSe cores in films of CdSe nanocrystals deposited electrophoretically can be used to examine elastic strain and strain relief by probing very thick films that have fractured. These and related measurements suggest that the in-plane elastic strain in these unfractured films can be as high as $\sim 2.5\%$ in the cores and $\sim 12\%$ overall in the film.

There is little known about the mechanical properties, such as the distribution of the residual stress and strain, stress relaxation, and fracture, of such nanocomponent films. Very little is also known about the interparticle bonding that occurs at the molecular level in these nanoparticle films and how it affects the more macroscopic mechanical properties of the film. Much of the understanding gained from these CdSe nanocrystal films is expected to be applicable to other nanocrystal thin films and can help establish conditions for the deposition of mechanically stable films suitable for practical applications.¹

In previous studies, the authors have shown that smooth, uniform films of CdSe nanocrystals can be formed by electrophoretic deposition of 3.2 nm diameter CdSe nanocrystals (prepared with TOPO (trioctylphosphine oxide) and TOPSe, and capped by TOPSe) from a hexane solution.^{2,3}

Seemingly identical films composed of distinct nanocrystals were deposited on both electrodes. No evidence of film cracking was observed for films thinner than $0.8 \mu\text{m}$, but channel cracking was seen in thicker films.²

In this study, films were electrophoretically deposited on planar electrodes (120-nm Au/10-nm Cr films on Si wafers) separated by 2 mm by using solutions of these CdSe nanocrystals (3.2 nm diameter cores, capped by TOPSe, ~ 555 nm first exciton absorption peak, ~ 565 nm luminescence peak) in hexane. Concentrations were typically 1×10^{15} nanoparticles/cm³ and the dc voltage was typically 500 V. Details can be found in refs 2 and 3.

No cracks were seen by using optical microscopy, atomic force microscopy (AFM), or scanning electron microscopy (SEM) for film thickness $< 0.8 \mu\text{m}$ for CdSe particle films. Evidence of channel cracks was seen for thicker films, 0.9 – $3.5 \mu\text{m}$ (Figure 1). This suggests that thinner, uncracked films are under tension. The thicker the film, the wider the cracks and the higher the density of cracks; hierarchical crack generation is suggested in the thicker films by the fracture patterns.

The different fracture patterns in the thinner and thicker films suggest that cracking occurs after deposition is complete. This was confirmed by optical microscopy of films that were partially removed from the solvent after deposition. No cracks were seen in the portion of the film remaining in solution. Cracks were observed for that part of the film out of solution within < 20 s of removal. Regions farther from the solution (and with a lower solvent vapor pressure) were more heavily cracked than those nearer the solution. These

* To whom correspondence should be addressed: e-mail, iph1@columbia.edu.

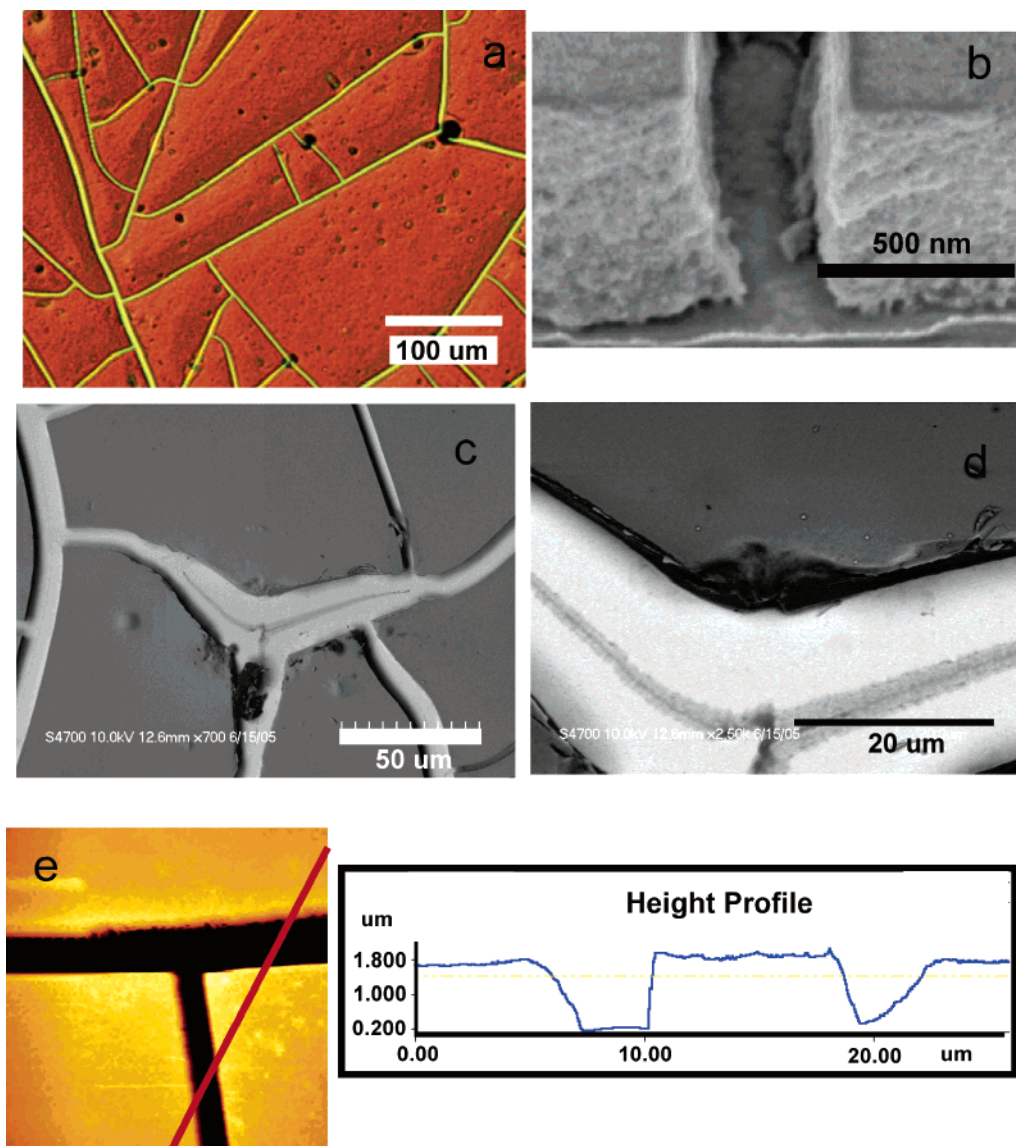


Figure 1. (a) Optical micrograph showing cracking in a $3.2 \mu\text{m}$ thick film of CdSe nanocrystals. Optical images were obtained with a Nikon Eclipse optical microscope equipped with an Insight digital camera in bright-field mode. The exposed regions in the cracks (which are dominated by a thin layer of nanocrystals overlaying the gold film substrate) appear as yellow lines. (b) SEM image showing delamination at a crack. (c) SEM of crack geometry, with brighter regions indicating a remnant thin film of CdSe nanocrystals on Au, whereas the darker regions indicate the delaminated CdSe nanocrystal film. (d) Higher magnification image of the cracked surface in (c). (b) is a secondary electron image obtained on a Hitachi S4700 field-emission SEM operated at 2 kV, while (c) and (d) are backscattered electron images obtained on a Hitachi S4700 field-emission SEM operated at 10 kV. (e) AFM image of a crack, with a trace across a crack edge at the right. Delamination is indicated by the raised edges of the film at the crack surface, as seen in the height profile. AFM images were obtained with a ThermoMicroscopes Autoprobe CP in tapping mode with 2 nm radius supersharp silicon tips with $k = 20\text{--}80 \text{ N/m}$ and also using d lever tips with $k = 1\text{--}3 \text{ N/m}$ (radius $<10 \text{ nm}$).

cracks creep toward the solvent meniscus but terminate before the meniscus. This is direct evidence that cracking occurs during drying, with the evaporation of residual solvent.

SEM and AFM analyses indicate that the cracks extend from the top of the film seemingly down to the Au film (Figure 1b, but this is not exactly so, as is seen below). Film delamination was observed by SEM, AFM, and—for wider cracks—by changes of reflected light on either side of the crack by optical microscopy. The channel cracks were typically $\sim 0.8\text{--}1.5 \mu\text{m}$ wide for $\sim 1 \mu\text{m}$ thick films and $\sim 4\text{--}25 \mu\text{m}$ wide for $\sim 3 \mu\text{m}$ thick films. The cracks are not always symmetric, especially near regions bounded by two channel

cracks. AFM and SEM showed the angle of delamination was $\lesssim 1.5^\circ$ for the thicker films and they were delaminated for $\sim 10 \mu\text{m}$ on either side of the crack (Figure 1b,e). The extent of delamination varied with the width of the crack as well with as the local geometry.

Raman microprobe measurements were made using the 488 nm line from an argon-ion laser in backscattering configuration. The spot size was $<3 \mu\text{m}$. Raman spectra using laser powers from $500 \mu\text{W}$ to 2 mW showed no evidence of heating, so laser powers were kept much below 1.5 mW and heating is not expected. Linearly polarized light was incident on the film, and both polarizations were collected. (Polarization effects should not be significant,

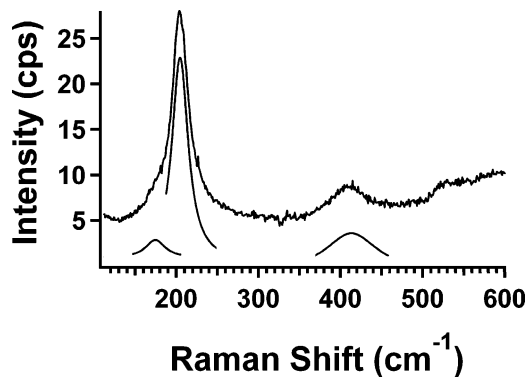


Figure 2. Representative Raman spectra of CdSe nanocrystals showing the Raman LO (210 cm^{-1}) and 2LO phonon (420 cm^{-1}) peaks, as well as that of the surface phonon (188 cm^{-1}). The peaks were fit to Lorentzian line shapes after subtracting a linear background.

given the likely random orientations of the nanocrystals.) At 488 nm there was some resonant enhancement for these 3.2 nm diameter particles ($\lambda_{\text{exciton}} = 555\text{ nm}$) and a weak luminescence background. Spectra were acquired across a crack—not always normal to the crack—and across regions where the channel cracks intersect.

Figure 2 shows a representative Raman spectrum of the $3.2\text{ }\mu\text{m}$ thick film, with contributions from the LO “bulk” phonons near 210 cm^{-1} and “surface” phonons near 188 cm^{-1} from the CdSe cores.^{4–6} Second-order “bulk” (2LO) peaks are also seen near 420 cm^{-1} . Raman traces are presented only for the LO “bulk” phonons; corresponding variations of Raman shifts with position are also seen for the LO surface and 2LO phonons and provide no additional information. The same peak intensity and shift are seen for traces taken forward and backward along a trajectory, suggesting there was no film damage during a scan—even in the delaminated regions.

Figure 3 plots the Raman peak intensities and shifts for scans near three different intersections of two channel cracks for a $3.2\text{ }\mu\text{m}$ thick film. The trace starts in the film, then proceeds across a crack, the tip of the film at the intersection of the crack, and another crack, and then proceeds into the film again. Within the crack/tip/crack region, the Raman intensity always decreases and sometimes shows a local maximum (Figure 3). At the tip, the Raman profile always shows a region where the shift increases relative to that in the film by $\delta_1 = 3.1 \pm 1.6\text{ cm}^{-1}$. Sometimes in the nearby channel cracks, the Raman shift decreases below that in the film by several cm^{-1} . The maximum overall increase in shift at the tip relative to the minimum in the trace is $\delta_2 = 6.4 \pm 1.5\text{ cm}^{-1}$.

The Raman intensity is expected to decrease in the crack/tip/crack region because presumably there is no film in the probed region. Although it seems reasonable that it does not decrease to zero because the beam size is finite ($\approx 3\text{ }\mu\text{m}$) and scanning is not normal to the cracks, there appears to be another reason for this. In much of the crack the exposed surface is not the Au layer but a very thin layer of CdSe nanocrystals atop the Au. As shown by energy dispersive X-ray analysis, the brighter regions in the crack in the SEMs

of parts c and d of Figure 1 and optical micrograph in Figure 1a (under higher magnification) are actually regions where this thin CdSe nanocrystal layer adheres to the Au surface (and survives delamination even with no surface adhesion treatment³), while the darker more central regions are exposed Au.

The increase in Raman shift at a tip shows that the in-plane strain and stress are relieved there more than at the films (as is seen below). The decrease in Raman shift seen in some of the cracks indicates there is little or no strain relief in the residual CdSe nanocrystal layer within the crack.

Scans across a single channel crack show a decrease in intensity in the crack and a decrease in Raman shift over most of the crack. There are also very localized regions where the shift increases in the crack.

The change in Raman shift in the CdSe cores is due to the strain felt by the cores, and this is treated using the model that describes how strain in zinc blende semiconductors affects phonon frequencies.⁷ (Although the structure of the CdSe cores is wurtzite, it has been approximated as being zinc blende because the structures are very similar.) The nanocrystals are assumed to be randomly oriented in the film, and the angle-averaged elastic modulus and Poisson’s ratio are used here.⁸ LO phonon backscattering is allowed from the zinc blende $\{100\}$ and $\{111\}$ planes, but not from the $\{110\}$ planes, so Raman signals are not obtained from all nanocrystals. Scattering from $\{111\}$ should be weighted much less than that from $\{100\}$ because the Raman scattering probability is smaller from $\{111\}$ by a factor of 3,⁹ and this more than compensates for the larger number of equivalent $\{111\}$ than $\{100\}$ planes (eight vs six). Consequently, only scattering from $\{100\}$ is analyzed.

In strained films, the frequency of phonons backscattering from the $\{100\}$ planes is¹⁰

$$\omega = \omega_0 + [p\epsilon_{zz} + q(\epsilon_{xx} + \epsilon_{yy})]/2\omega_0 \quad (1)$$

where ω_0 is the frequency from unstrained CdSe nanocrystals and p and q are the phonon deformation potentials;⁷ these have been approximated as $-\omega_{\text{LO}}^2$ and $-1.8\omega_{\text{LO}}^2$, respectively, for bulk semiconductors (with $\omega_0 = \omega_{\text{LO}}$ here).^{7,11} This gives a Gruneisen parameter

$$\gamma = -(p + 2q)/6\omega_0^2 \quad (2)$$

of ~ 0.77 , which is consistent with that expected for a 3.2 nm diameter CdSe nanocrystal.¹²

Assuming plane stress in an unrelaxed $\{100\}$ film structure, the isotropic in-plane strain is $\epsilon_{xx} = \epsilon_{yy} = \epsilon$ and the isotropic in-plane stress is $\sigma_{xx} = \sigma_{yy} = \sigma$. With the normal stress $\sigma_{zz} = 0$, it follows that $\epsilon_{zz} = -[2\nu/(1 - \nu)]\epsilon$, where ν is Poisson’s ratio.¹³ In the delaminated region near a channel crack, stress is expected to be relieved in the direction normal to the crack (say in the y direction), but not in the direction parallel to it (the x direction), and so $\sigma_{yy} = \sigma_{zz} = 0$. The expectation that σ_{xx} in the delaminated region should be the same as that in the strained regions, σ , gives $\epsilon_{xx} = \epsilon/(1 - \nu)$

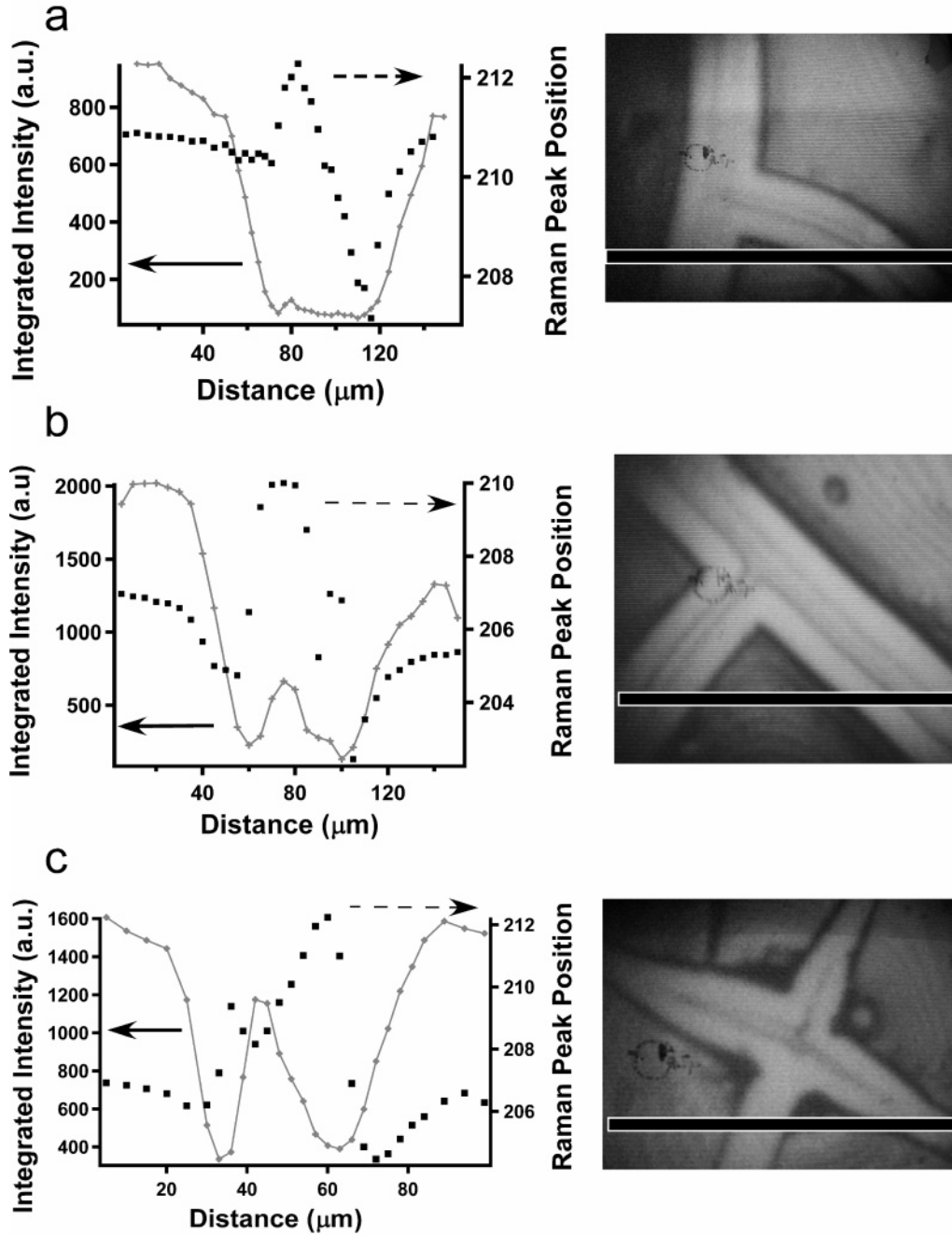


Figure 3. (a–c) Integrated intensity and peak shift of Raman traces (left panels) and corresponding optical micrographs (right panels) across cracks in $3.2 \mu\text{m}$ thick electrophoretically deposited CdSe nanocrystal films. In each panel, the left axis (integrated intensity) corresponds to the trace with the lines and markers; the right axis (Raman peak position) corresponds to the trace with square markers. The traces extend beyond the region shown in the images.

and $\epsilon_{yy} = \epsilon_{zz} = -[\nu/(1 - \nu)]\epsilon$. In the delaminated film tip where two channel cracks cross, there is total stress relaxation and strain relief and $\epsilon_{xx} = \epsilon_{yy} = \epsilon_{zz} = 0$.¹³

For phonon backscattering from $\{100\}$

$$\omega = \omega_0 + [q - p\nu/(1 - \nu)]\epsilon/\omega_0 \quad (3)$$

in the fully strained regions and

$$\omega = \omega_0 + [q - p\nu/(1 - \nu)]\epsilon/2\omega_0 \quad (4)$$

in the partially relaxed delaminated regions near a channel crack and ω_0 in the totally relaxed regions where the channel cracks intersect. The Raman shift is larger in the fully relaxed cracked regions, relative to unrelaxed regions, by $258\epsilon \text{ cm}^{-1}$ ($=\delta_2$) and by half that in the partially relaxed regions ($=\delta_1$). (This is determined using p and q from above, $\omega_0 = 213 \text{ cm}^{-1}$, and $\nu = 0.37$.⁸ See Supporting Information.) Therefore, it is expected that $\delta_2 = 2\delta_1$; this relation is consistent with the Raman shift measurements. (Note, however, that the run-to-run values are more consistent for δ_2 . The larger observed variations in δ_1 may be due to curvature of the crack flanks,

which would lead to a small nonzero value of σ_{yy} and a concomitant change in σ_{xx} that would alter the values of ϵ_{xx} and ϵ_{yy} . The Raman shift that provides δ_1 would be a function of the magnitude and sign of curvature of the crack flanks and could vary along the crack flank and be different on opposing sides of a crack.) The Raman shift $\delta_2 = 6.4 \text{ cm}^{-1}$ suggests a decrease of the in-plane elastic strain in the CdSe nanocrystal cores of $\epsilon \sim 2.5\%$ from fully (tensile) strained to fully strain-relieved regions. (Reference 5 suggests that the Raman shift is linear with strain in this regime, as has been assumed.)

Because the optical phonon frequencies decrease with increasing temperature, any laser heating would decrease the Raman shift. This is exactly the opposite of what is seen, with the observed increased shifts occurring at the most likely possible sites of heating, such as at the delaminated tips of the already thermally insulating film, and observed decreased shifts at sites where very little laser heating would be expected, such as at the residual, very thin nanocrystal layer adhering to the highly thermally conductive Au layer.

These CdSe nanocrystals were also electrophoretically deposited on patterned gold stripe electrodes, 10–50 μm wide, as in ref 2.² In some cases, SEM showed an asymmetry in morphology that suggests poor morphology and poor adhesion on the “right” edge (inset to Figure 4b). There is also an increase in Raman shift at the edge by $\sim 6 \text{ cm}^{-1}$ (Figure 4a,b), which is consistent with interpreting such an increase to a transition from fully strained to strain-relieved regions.

The overall strain in the unrelaxed films is estimated by examining the cracks and delaminated regions in the fracture patterns in the relaxed films. This assumes that the measurements of the widths of the crack and delamination regions are not affected by the delamination; this is true because the delamination angle is very small (of $\lesssim 1.5^\circ$). If a channel crack has a width b and the film has delaminated a distance a on either side (as determined optically, as above), the overall in-plane film tensile strain before cracking is $\epsilon = b/(2a + b)$. For the 3.2 μm thick film, the cracks have widths varying from 4 to 10 μm and delamination widths ranging from 20 to 25 μm , giving an area-averaged in-plane tensile strain of $\sim 11.7\%$ before relaxation.

The Raman shifts depend on the strain in the CdSe cores ($\sim 2.5\%$ here), which is likely different than the strain in the TOPO ligand regions and the overall strain in this film ($\sim 11.7\%$ here). Knowing these two quantities further allows us to determine other mechanical parameters for the films.¹ (See Supporting Information.) Under conditions of plane stress (with in-plane stress σ), σ/ϵ is the biaxial modulus = $E/(1 - \nu)$, where E is the elastic modulus and ν is Poisson’s ratio. The value of σ should be the same for the film itself and its components. Using the averaged bulk values for CdSe, $E_{\text{CdSe}} = 41.5 \text{ GPa}$ and $\nu_{\text{CdSe}} = 0.37$,^{8,14} the biaxial modulus of the core is $E_{\text{CdSe}}/(1 - \nu_{\text{CdSe}}) = 65.9 \text{ GPa}$. The in-plane stress is $\sigma = (0.025)(65.9 \text{ GPa}) = 1.6 \text{ GPa}$. Moreover, $E_{\text{film}}/(1 - \nu_{\text{film}}) = (0.025/0.117)E_{\text{CdSe}}/(1 - \nu_{\text{CdSe}}) = 0.21E_{\text{CdSe}}/(1 - \nu_{\text{CdSe}}) \sim 13.8 \text{ GPa}$.

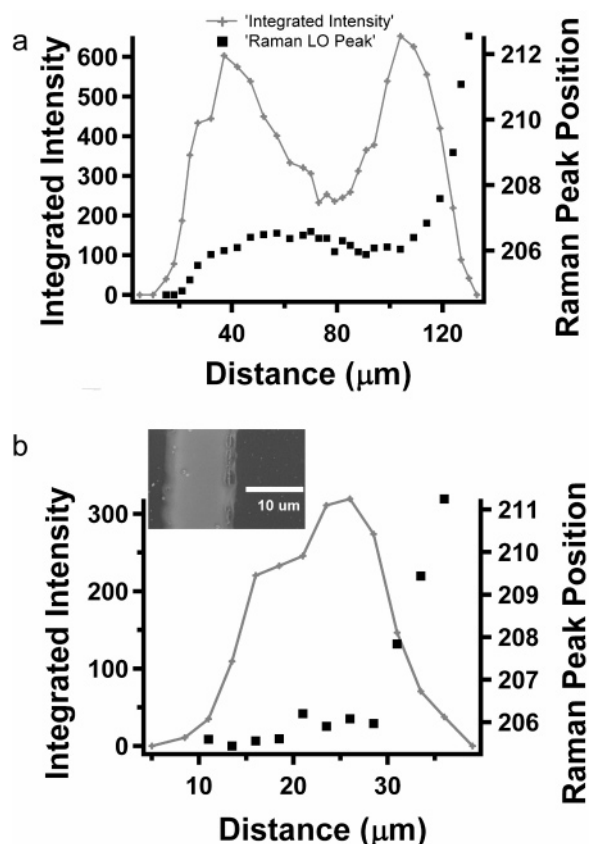


Figure 4. Raman traces across bars of electrophoretically deposited CdSe nanocrystals that are nominally (a) $\sim 50 \mu\text{m}$ and (b) $\sim 10 \mu\text{m}$ wide and 600 nm thick. Asymmetry in the Raman plot is evident, with the higher frequency Raman peaks occurring on the same side of the bars. The inset to (b) is an SEM image showing delamination of the nanocrystal film on the right side of the 10 μm wide bar. (Delamination at the right side is also seen for the 50 μm wide bar.)

It is assumed that the CdSe/TOPO nanoparticles (3.2 nm diameter CdSe core and overall 4.5 nm diameter) are packed closely with no voids, with ligands occupying the interstitial regions, so the CdSe cores occupy a fraction $\rho = 0.43$ of the volume and the ligands the remaining $1 - \rho = 0.57$. Micromechanics models are applied to the films with spherical inclusions (CdSe cores) in a matrix (TOPO ligands).¹⁵ It is first assumed that the biaxial modulus of CdSe is much larger than that of the effective TOPO ligand matrix, and so $E_{\text{CdSe}} \gg E_{\text{TOPO}}$, and this assumption is subsequently verified for self-consistency. The various mechanical moduli (bulk, shear, and so on) scale the same way in several of these models and differently in others.

In this limit, and for reasonable ranges of uncertain parameters, the micromechanics models give $[E_{\text{film}}/(1 - \nu_{\text{film}})]/[E_{\text{TOPO}}/(1 - \nu_{\text{TOPO}})]$ of about 2.75. (This ratio is 3.26 (for the Halpin–Tsai equation with $\xi = 2$),¹⁶ 2.75 (for the Cohen–Ishai equation),¹⁷ 2.33–2.65 (for the Mori–Tanaka method),¹⁸ and 1.75–2.76 (for the ratio of film and TOPO bulk moduli for the Christiansen–Luo generalized self-consistent method).¹⁸ See Supporting Information.) Using $E_{\text{TOPO}}/(1 - \nu_{\text{TOPO}}) = 0.36E_{\text{film}}/(1 - \nu_{\text{film}})$, the effective biaxial modulus for TOPO in these films is $E_{\text{TOPO}}/(1 - \nu_{\text{TOPO}}) = 0.077E_{\text{CdSe}}/(1 - \nu_{\text{CdSe}}) \sim 5.1 \text{ GPa}$. This effective elastic

modulus is $1 - \nu_{\text{TOPO}} \sim 0\text{--}40\%$ smaller than this ($\sim 3\text{--}5$ GPa) and can be compared to the elastic moduli of polystyrene, 3.8 GPa, solid dodecane, ~ 1 GPa,^{19,20} polypropylene, 1.5–2.0 GPa, polyethylene terephthalate, 2.0–2.5 GPa, and nylon, 2–4 GPa.

These micromechanics models predict that $E_{\text{film}}/E_{\text{TOPO}}$ diverges as ρ approaches 1 (as $1/(1 - \rho)$ for first, third, and fourth models and as $1/(1 - \rho^{1/3})$ for the second model), meaning that for high loading factors they approach (at least a fraction of) E_{CdSe} . A more recent model²¹ is appealing in that it addresses disordered monodisperse spherical inclusions (such as the monodisperse CdSe cores) in a random matrix, and predicts that $E_{\text{film}}/E_{\text{TOPO}}$ diverges as $1/(1 - 2\rho)$ as ρ approaches 0.5. For $\rho = 0.43$, this gives $[E_{\text{film}}/(1 - \nu_{\text{film}})]/[E_{\text{TOPO}}/(1 - \nu_{\text{TOPO}})] = 4.0, 9.1, \text{ and } 8.7$ for $\nu_{\text{film}} = 0.1, 0.33, \text{ and } 0.5$, respectively, which is much higher than the above model predictions and would give a much smaller biaxial modulus for the TOPO. However, the assumption of a random mixture of inclusions and matrix is not valid because the TOPO matrix is presumably bound to the surfaces of the CdSe cores.

Fracture occurs at the ligands, because bonding between the ligands on neighboring particles is likely weaker than that between the ligands and the core, which in turn is likely weaker than that between the atoms in the core. Because much of the exposed surface in the cracks is not that of the Au beneath the nanocrystal film, but a very thin layer of CdSe nanocrystals, fracture involving the ligands is important both in the sidewalls of the crack and in the delamination from the surface. Clearly, microscopic models of the elastic constants and fracture of composite materials are not totally adequate in describing this fracture. A nanoscopic model is needed, which includes the ligand density, interdigitation, and ligand-to-core bonding strength.

The uncertainties in the elastic strains and biaxial moduli obtained here depend on several factors in addition to the validity of the micromechanics models. For example, there are uncertainties in the phonon deformation potentials, which become significant because the perturbations in the core phonon frequency from in-plane and normal-to-plane strain partially cancel. Also, the mechanical properties of the CdSe cores are only approximately equal to those of bulk CdSe. Furthermore, each material component has been assumed to be elastic and harmonic.

In conclusion, Raman microprobe analysis is shown to be a particularly appropriate technique for studying elastic strain in the cores of nanocrystal films, especially for very small nanocrystals when the Debye–Scherrer broadening in X-ray diffraction is very large. When combined with other methods, Raman microprobe analysis provides valuable information, which can lead to better understanding of mechanical properties on micro- and nanodimension levels and improved methods for fabricating nanocomponent films. Notably, large strains are seen to develop in the cores of nanocrystals due to solvent evaporation and the films fracture with the concomitant large film strain; this is important for the electrochemically deposited films studied here, as well as for dry cast films, for which solvent evaporation is also important.

These are the first measurements of the mechanical properties of ensembles of quantum dots and are likely relevant to understanding most aggregates and assemblies of nanoparticles; they underline some of the challenges associated with obtaining mechanically robust assemblies of nanocrystals. Further, this analysis shows how to use micromechanics models to analyze such complex nanoscale systems and shows the importance of improving such models.

Acknowledgment. This work was supported primarily by the MRSEC Program of the National Science Foundation under Award Number DMR-0213574 and the New York State Office of Science, Technology and Academic Research (NYSTAR), and partially by the NSEC Program of the National Science Foundation under Award Number CHE-0117752 and the National Science Foundation under Award Number CMS-0134226. The authors warmly acknowledge useful conversations with Yigal Komem and I. Cev Noyan, contributions in preliminary studies from Ben Smith and Mohammad Islam, and technical help from Richard Harniman.

Supporting Information Available: Descriptions of strain and biaxial modulus of CdSe cores in nanocrystal films and micromechanics models. This material is available free of charge via the Internet at <http://pubs.acs.org>.

References

- Freund, L. B.; Suresh, S. *Thin Film Materials: Stress, Defect Formation, and Surface Evolution*; Cambridge University Press: Cambridge, 2003; Vol. 1.
- Islam, M. A.; Herman, I. P. *Appl. Phys. Lett.* **2002**, *80* (20), 3823.
- Islam, M. A.; Xia, Y.; Telesca, D. A., Jr.; Steigerwald, M. L.; Herman, I. P. *Chem. Mater.* **2004**, *16* (1), 49.
- Alivisatos, A. P.; Harris, T. D.; Carroll, P. J.; Steigerwald, M. L.; Brus, L. E. *J. Chem. Phys.* **1989**, *90* (7), 3463.
- Alivisatos, A. P.; Harris, T. D.; Brus, L. E.; Jayaraman, A. *J. Chem. Phys.* **1988**, *89* (10), 5979.
- Hwang, Y.-N.; Park, S.-H.; Kim, D. *Phys. Rev. B* **1999**, *59* (11), 7285.
- Geurts, J. *Prog. Crystal Growth and Charact.* **1996**, *32*, 185.
- Simmons, G.; Wang, H. *Single-Crystal Elastic Constants and Calculated Aggregate Properties: A Handbook*, 2nd ed.; M.I.T. Press: Cambridge, MA, 1971.
- Pollak, F. In *Analytical Raman Spectroscopy*; Grasselli, J. G., Bulkin, B. J., Eds.; John Wiley and Sons, Inc.: New York, 1991.
- Anastassakis, E.; Pinczuk, A.; Burstein, E.; Pollak, F. H.; Cardona, M. *Solid State Commun.* **1970**, *8*, 133.
- Dinger, A.; Hetterich, M.; Goppert, M.; Grun, M.; Klingshir, C.; Weise, B.; Liang, J.; Wagner, V.; Geurts, J. *J. Cryst. Growth* **1999**, *200*, 391.
- Meulenberg, R. W.; Strouse, G. F. *Phys. Rev. B* **2002**, *66*, 035317.
- Timoshenko, S. P.; Goodier, J. N. *Theory of Elasticity*; McGraw-Hill: New York, 1987.
- Cline, C. F.; Dunegan, H. L.; Henderson, G. W. *J. Appl. Phys.* **1967**, *38*, 1944.
- Halpin, J. C. *Primer on Composite Materials Analysis*, 2nd ed.; CRC Press: Boca Raton, FL, 1992.
- Halpin, J. C.; Kardos, J. L. *Polym. Eng. Sci.* **1976**, *16* (5), 344.
- Cohen, L. J.; Ishai, O. *J. Composite Mat.* **1967**, *1*, 390.
- Christensen, R. M. *J. Mech. Phys. Solids* **1990**, *38* (3), 379.
- Mason, W. P. *American Institute of Physics Handbook*, 3rd ed.; McGraw-Hill: New York, 1972.
- Dymond, J. H.; Robertson, J.; Isdale, J. D. *J. Chem. Thermodyn.* **1982**, *14*, 51.
- Christensen, R. M. *Composites, Part B* **2004**, *35*, 475.

NL051921G